Skeletal dosimetry for external exposure to photons based on μCT images of spongiosa from different bone sites

R Kramer [1], H J Khoury [1], J W Vieira [2, 3] and I Kawrakow [4]

[1] Departamento de Energia Nuclear, Universidade Federal de Pernambuco, Av. Prof. Luiz Freire 1000, Cidade Universitária, CEP 50740-540, Recife, PE, Brazil

[2] Centro Federal de Educação Tecnológica de Pernambuco, Recife, PE, Brazil

[3] Escola Politécnica, UPE, Recife, PE, Brazil

[4] Ionizing Radiation Standards, National Research Council of Canada, Ottawa, Canada

E-mail: rkramer@uol.com.br

Statement of provenance:
'This is an author-created, un-copyedited version of an article accepted for publication in Physics in Medicine and Biology. IOP Publishing Ltd is not responsible for any errors or omissions in this version of the manuscript or any version derived from it. The definitive publisher authenticated version is available at doi:10.1088/0031-9155/52/22/010. '

ABSTRACT

Micro Computed Tomography (μCT) images of human spongiosa have recently been used for skeletal dosimetry with respect to external exposure to photon radiation. In this previous investigation, the calculation of equivalent dose to the red bone marrow (RBM) and to the bone surface cells (BSC) was based on five different clusters of micro matrices derived from μCT images of vertebrae and the BSC equivalent dose for 10 μm thickness of the BSC layer was determined using an extrapolation method. The purpose of this study is to extend the earlier investigation by using μCT images from eight different bone sites and by introducing an algorithm for the direct calculation of the BSC equivalent dose with sub-micro voxel resolution. The results show that for given trabecular bone volume fractions (TBVFs) the whole-body RBM equivalent dose does not depend on bone site-specific properties or imaging parameters. However, this study demonstrates that apart from the TBVF and the BSC layer thickness, the BSC equivalent dose additionally depends on a so-called "trabecular bone structure (TBS) effect", i.e. that the contribution of photo-electrons released in trabecular bone to the BSC equivalent dose depends also on the bone site-specific structure of the trabeculae. For a given bone site, the TBS effect is also a function of the thickness of the BSC layer and it could be shown that this effect would disappear almost completely, should the BSC layer thickness be raised from 10 to 50 μm, according to new radiobiological findings.

1. Introduction

1.1 The skeletal tissues at risk

The determination of equivalent dose to radiosensitive skeletal soft tissues is one of the most challenging tasks in dosimetry, because these soft tissues, the haematopoietic stem cells of the marrow, called "red bone marrow" (RBM), and the osteogenic cells on the endosteal surfaces, called "bone surface cells" (BSC) or bone endosteum, are located in the irregularly shaped marrow cavities of trabecular bone with diameters ranging from 50 to 2000 μm (Spiers 1969). "Trabecular bone plus its supported soft tissue is sometimes also referred to as spongiosa" (ICRP 1995).

The BSC represent the part of the marrow volume that is located within a distance of 10 μm from the surfaces of mainly trabecular bone (ICRP 1979), while the RBM occupies a part of the remaining marrow volume given by the cellularity factor (ICRP 1995). BSC can also be found on the surfaces of cortical bone, but "because cell proliferation is greater on trabecular than on cortical surfaces, it is to be expected that malignant transformation will occur more readily in the endosteum of trabecular bone" (Spiers 1974). Discussion about the location and the distribution of the two skeletal tissues at risk is still ongoing with respect to the revision of the thickness of the BSC layer from 10 to 50 μm, the exclusion of the Haversian canals of cortical bone, the inclusion of cortical surfaces of the medullary cavities (Bolch et al 2007), the consideration of trabecular bone remodelling (Richardson et al 2007) and the inhomogeneous distribution of RBM cells in the marrow (Watchman et al 2007a).

1.2 Previous investigations of skeletal dosimetry based on micro Computed Tomography (μCT) images of spongiosa

Digital μCT or NMR images of human spongiosa for the purposes of skeletal dosimetry were introduced by W.Bolch and co-workers from the University of Florida (Jokisch et al 1998, Jokisch et al 2001, Bolch et al 2002, Patton et al 2002, Rajon et al 2002, Shah et al 2003, Shah et al 2005a,b,c,d). In these studies, samples from various bone sites of human skeletons were scanned by micro CT or NMR, the resulting images were segmented into trabecular bone and marrow, and then introduced first into the EGS4 Monte Carlo (MC) code (Nelson et al 1985), and later into the EGSnrc MC code (Kawrakow 2000a), employing a special algorithm called PIRT ("paired-image radiation transport"). In the PIRT method particles are transported through a "macro" matrix with a voxel size of some hundred μm, representing spongiosa, cortical bone and surrounding soft tissues, and at the same time through a "micro" matrix with cubic voxel sizes down to 30 μm, representing the micro structure of spongiosa with segmented volumes of marrow and trabecular bone. So far this method has mainly been applied to nuclear medicine applications and only to isolated bone samples, but not to a complete skeleton embedded in a human body.

μCT image-based calculations of equivalent dose to the RBM and the BSC from external exposure to photon radiation for complete skeletons embedded in human bodies have been published recently for the first time (Kramer et al 2006b), from here on referred to as FM ("first micro") paper. This became possible due to the segmentation of spongiosa in the skeletons of the MAX06 and the FAX06 phantoms (Kramer et al 2006a), due to the use of segmented μCT images of trabecular bone, and due to the 8R cluster method introduced in the FM paper. The 8R cluster method is an algorithm especially developed to employ only the minimum amount of trabecular microstructure information necessary to describe the spongiosa voxels at runtime (Kramer et al 2006b). For external exposure to photons the μCT image-based 8R cluster approach demonstrated that previous investigations overestimated the RBM and BSC equivalent doses. This over-prediction is mainly due to the use of skeletons made of a homogeneous mixture of bone and marrow, in which the cortical bone layer becomes contributor to the equivalent dose instead of acting as a shielding for the underlying spongiosa, and for high energies additionally because of the use of the kerma approximation which ignores the secondary electron escape from the spongiosa volume.

1.3 The purpose of this study

In the FM paper, the equivalent dose to the BSC for a thickness of 10 μm was determined using an extrapolation method based on the results obtained for thickness of 17.65, 30 and 60 μm according to the cubic voxel resolutions of 17.65, 30 and 60 μm of the μCT images. The principal limitation of this method is that no reliable estimate of the systematic uncertainty of the extrapolation is possible. An additional, practical limitation of the approach is the need for at least three different micro voxel resolutions. A third limitation of the previous investigation reported in the FM paper is the fact that the micro structure information for a given voxel resolution was obtained from one vertebra sample by

modifying the images to achieve the required trabecular bone volume fraction (TBVF). This limitation was caused by the lack of μCT images from bone sites other than vertebrae at the time of the previous investigation. As new μCT images for other bone sites became available, the vertebra-based approach can now be extended.

The purpose of this study is therefore

- to develop and use an algorithm for the direct calculation of the equivalent dose to the BSC layer on a sub-micro voxel scale, and
- to investigate the dependence of the RBM and the BSC equivalent dose for external exposure to photons on the voxel resolution, on the segmentation method, on the TBVF and on the type of bone site.

2. Materials and Methods

2.1 The MAX06 and the FAX06 phantoms

The MAX06 and FAX06 phantoms (Kramer et al 2006a) are utilized in this study. MAX06 and FAX06 are updated versions of the MAX (Kramer et al 2003) and of the FAX phantoms (Kramer et al 2004) that include the extrathorarcic airways, the oral mucosa, the gall bladder, the heart, the lymphatic nodes, the prostate and the salivary glands according to the revised effective dose concept (ICRP 2007), and also provide separately segmented regions of cortical bone, spongiosa, medullary yellow marrow and cartilage, thus permitting the use μCT spongiosa images for skeletal dosimetry. The updated phantoms are made of 1.2 mm cubic voxel, and the additional segmentation was based on the original CT images from which the MAX/FAX phantoms were developed, on anatomical textbooks, and on skeletal data provided by ICRP70 (ICRP 1995) and ICRP89 (ICRP 2002). Like MAX and FAX, the MAX06 and the FAX06 phantoms have organ and soft tissue masses in accordance with the reference data from ICRP89, but in addition skeletal tissue volumes based on ICRP89 and ICRP70. Tissue densities were taken from ICRU Reports 44 and 46 (ICRU 1989, 1992). The complete description of the MAX06 and the FAX06 phantoms can be found elsewhere (Kramer et al 2006a). In order to keep this paper to a reasonable length, only results based on the FAX06 phantom are included. When using the same spongiosa micro matrices, RBM and BSC equivalent doses for the MAX06 phantom are very similar.

2.2 The μCT images

Table 1 presents information as far as available about the bone specimens and about the individuals from which the samples have been taken post mortem. These μCT images of spongiosa have been provided by Salmon (2006), specimen S0117, by Bolch (Shah et al 2005c), specimens B0160 and B0260, and by Bauer (Bauer et al 2004), all other specimens. The bone specimens were obtained from donors with no medical history of metabolic bone disease or cancer and showed no radiographic evidence of damage or bone pathologies. Introducing the μCT images into the 1.2mm cubic macro voxels of the FAX06 phantom's spongiosa requires so-called micro matrices to be extracted from the images, which are 1.2mm cubes filled with segmented micro voxels of trabecular bone and marrow.

Specimen **B0260** arrived as a parallelepiped of spongiosa with dimensions of 22.8 mm x 17.1 mm x 4.2 mm extracted from the frontal part of the skull which was then segmented into trabecular bone and marrow. The segmentation process included the following steps (Rajon et al 2006):

- median filtration with kernel size 3x3x3 to remove noise,
- thresholding using image-gradient inspection
- segmentation into binary images of trabecular bone and soft tissue.

The micro matrix dimensions based on specimen B0260 were 20 x 20 x 20.

Table 1. Specifications of the μCT images of spongiosa

Bone Specimen	Gender	Age [y]	Height [cm]	Weight [kg]	Bone	TBVF [%]	Image size [mm^3]	Resolution [μm]
S0117					11. Thor. vertebra	17.5	9.0 x 9.0 x 4.5	17.65
B1830	female	68	170	70	8. Thor. vertebra	16.2	7.9 x 7.9 x 7.7	30
B0160	male	66	173	68	4. Lum. vertebra	22.9	12.0 x 12.9 x 8.7	60
B0260	male	66	173	68	Frontal skull	40.4	22.8 x 17.1 x 4.2	60
B2026	male	64	176	76	10. Thor. vertebra	14.0	6.7 x 6.7 x 6.0	26
B2126	male	64	176	76	2. Lum. vertebra	10.2	6.7 x 6.7 x 6.0	26
B2226	male	64	176	76	Femur neck	15.6	6.7 x 6.7 x 6.0	26
B1326	male	80	162	49	Iliac crest	7.4	13.3 x 13.3 x 6.0	26

TBVF: Trabecular Bone Volume Fraction
Thor: thorarcic
Lum: lumbar

232 raw images with 26 μm voxel resolution have been received for each of the specimens **B2026-B2226** with 256 pixel x 256 pixel each and for specimen **B1326** with 512 pixel x 512 pixel. The images have been rescaled to a voxel resolution of 26.087 μm in order to yield a micro matrix dimension of 46 x 46 x 46. After the removal of noise with a median filter (kernel size 3x3x3), the images were segmented into trabecular bone and marrow by using the histogram-based threshold function of the SCION imaging software (SCION 2000). Finally parallelepipeds of spongiosa with a size of 6.7 mm x 6.7 mm x 6.0 mm and 13.3 mm x 13.3 mm x 6.0 mm have been extracted from the segmented images B2026-2226 and B1326, respectively.

Segmentation of the first three specimens in table 3 occurred with similar methods and was already described in the FM paper.

2.3 Skeletal dosimetry with a cluster of micro matrices

The 8R cluster method was introduced for the calculation of RBM and BSC equivalent doses in the MAX06 and the FAX06 phantoms for external exposure to photons, based on a cluster of 8 micro matrices containing segmented BSC voxels located between trabecular bone and marrow voxels (Kramer et al 2006b). When a particle enters a spongiosa voxel, one of the 8 micro matrices is randomly chosen and the particle transport then occurs in that micro matrix. Continuation in a neighbouring spongiosa voxel triggers a new random selection of a micro matrix from the cluster, etc. until the particle leaves the spongiosa and enters the cortical bone shell, where the transport is then re-transferred to the phantom's macro matrix made of 1.2mm cubic voxels.
The cluster of micro matrices can also be applied in a systematic-periodic manner. On entry into the spongiosa, the first micro matrix of the cluster is selected for transport. Continuation in a neighbouring spongiosa voxel occurs in the neighbouring micro matrix in the cluster, and, if necessary, the cluster as a whole is repeated to guarantee continuous transport through the spongiosa. Compared to the random selection of micro matrices, the systematic-periodic cluster method preserves coherently the cluster of spongiosa during transport. Care is taken that the TBFVs of the clusters correspond to the TBVFs of the images from which they have been extracted. For a complete description of the cluster method the reader is kindly referred to the FM paper (Kramer et al 2006b).

2.4 Micro clusters for different TBVFs and bone sites

The amount of bone tissue contained in the spongiosa can vary significantly among different bones, different individuals and different age groups. Table 1 shows variations of the TBVF among the five vertebrae between 10.2 and 22.9%. The 7.4% TBVF observed for the iliac crest is a rather low value, but can occur for older people because of natural bone loss, while for younger individuals the iliac crest has usually a TBVF of ca. 20%. TBVFs for the most important human bones can be found in table 15 of ICRP Publication 70 (ICRP 1995), whose rounded values are reproduced in table 2, which apply to adults of age 41 to 50.

Table 2. Trabecular bone volume fractions based on ICRP Publication 70 (ICRP 1995)

Adult Skeletal region	TBVF %
Arm bones	15
Ribcage	10
Spine	12
Skull	55
Mandible	55
Pelvis	20
Leg bones	15

The micro sets utilized in this investigation are summarized in Table 3. A set is represented by five micro clusters, each of which has a specific TBVF and is composed of 8 or 27 micro matrices. The first three rows of the table (17.65mv, 30mv, 60mv) list the sets already employed in the FM paper.

Table 3. Micro sets used for the calculations

			ribcage		spine		longbones		pelvis		skull/mandible	
Micro set	Resolution [μm]	nmic	TBVF %	cluster type	TBVF %	cluster type	TBVF %	cluster type	TBVF %	cluster type	TBVF %	cluster type
17.65mv	17.65	8	10	mv	12	mv	15	mv	20	mv	55	mv
30mv	30	8	10	mv	12	mv	15	mv	20	mv	55	mv
60mv	60	8	10	mv	12	mv	15	mv	20	mv	55	mv
60ms	60	8	10	ms	12	ms	15	ms	20	ms	55	ms
26o1	26	8	10	mv1	14	orig1	15.6	orig	7.4	orig	55	mv1
26o2	26	8	10	mv2	10.2	orig2	15.6	orig	7.4	orig	55	mv2
26mv1	26	8	10	mv1	12	mv1	15	mv1	20	mv1	55	mv1
26mv2	26	8	10	mv2	12	mv2	15	mv2	20	mv2	55	mv2
26mv1p	26	8	10	mv1	12	mv1	15	mv1	20	mp	55	mv1
26mv2p	26	8	10	mv2	12	mv2	15	mv2	20	mp	55	mv2
26mv1_27	26	27	10	mv1	12	mv1	15	mv1	20	mv1	55	mv1
26mv2_27	26	27	10	mv2	12	mv2	15	mv2	20	mv2	55	mv2

TBVF: Trabecular bone volume fraction
nmic: number of micro matrices in the cluster.
mv: modified vertebra image.
ms: modified skull image.
mp: modified pelvis image
orig: original image

The cluster types labelled as “mv”, “ms” and “mp” were obtained by modifying the original images of a vertebra, the skull or the pelvis, respectively, to produce the TBVFs given in table 2. The modification of the images was performed with an algorithm, which uniformly adds/removes trabecular bone voxels to/from the trabecular surfaces until the desired TBVF is achieved. Cluster types denoted “orig” represent micro clusters which have the original TBVFs mentioned in table 1, while the numbers “1” and “2” are used to distinguish between vertebra B2026 and B2126, respectively.

2.5 A new BSC algorithm

In this study, the BSC volume is considered to be a 10 μm thick layer on all surfaces of trabecular bone and additionally on those surfaces of cortical bone, which are in contact with spongiosa. All calculations reported here were performed with a user code, called “fax06_egsnrc”, based on the EGSnrc Monte Carlo system (Kawrakow 2000a,b, 2003, 2006) and described in the FM paper (Kramer et al 2006b). For the purposes of this investigation the fax06_egsnrc code was modified to permit the computation of BSC equivalent dose in unsegmented sub-volumes of micro voxels. In the original implementation, micro matrices were segmented into trabecular bone (TB), bone marrow (BM) and BSC voxels. In this study, micro matrices are only segmented into TB and BM voxels. Thus, for the calculation of BSC equivalent dose two problems had to be solved: The division of the energy to be deposited between the BSC and the BM sub-volumes within a micro voxel and the correct representation of BSC layers in systematically-periodically repeated micro matrices and clusters.

2.5.1 Energy deposition in sub-volumes of a micro voxel

For energy deposition events in BM micro voxels at run time, the new algorithm checks if the voxel has one or more TB neighbours or if it is adjacent to a cortical bone macro voxel. If not, the entire energy is scored to the RBM equivalent dose, taking into account the cellularity factor for the corresponding bone. If yes, a fraction of the volume in the BM voxel is considered to be a BSC layer and consequently the energy deposited must be distributed between the BM and the BSC sub-volumes. The main problem of the calculation of fractions of energy to be deposited in BM and BSC sub-volumes comes from the fact that EGSnrc and all other general-purpose codes use the condensed history technique for charged particle transport (Berger 1963). This is necessary because charged particles interact at a very high rate and therefore analogue (i.e. event-by-event) simulation is not practical in most cases due to the excessively long calculation times required. The condensed history method therefore combines many individual transport and collision processes into a single „step“, determining changes of the particle’s energy, position and direction from appropriate multiple scattering theories at the end of the step. Thus, only the initial and final position, the direction and the energy lost in the step are known, but not the details of the curved path that connects the two endpoints of the step. One must therefore devise an algorithm for distributing the energy between the initial and final position of the step. The simplest possible approach is to connect the two endpoints with a straight line and to assign fractions of energy to the two sub-volumes based on the line segment falling into them as indicated in figure 1a. However, this may result in inaccurate estimates as indicated in figure 1b.

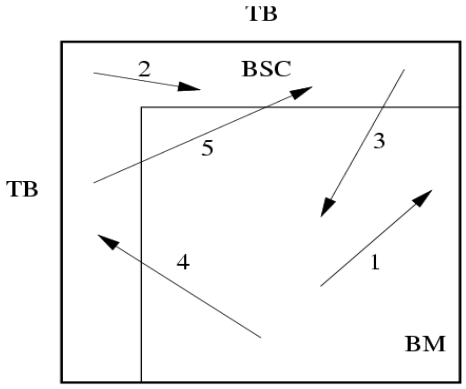

Figure 1a. Five electron trajectories in a bone marrow (BM) micro voxel that has a BSC layer adjacent to trabecular bone (TB). For trajectory 1, which starts and ends in BM, the entire energy is scored into RBM. In a similar way, the entire energy deposited by trajectory 2 is collected as a contribution to the BSC equivalent dose. For trajectories 3 (starts in BSC, ends in BM) and 4 (starts in BM, ends in BSC), the energy is divided between RBM and BSC according to the path-length in the two sub-volumes. Even for trajectories such as 5, which starts in BSC, traverses the BM volume, and ends in BSC, the contributions to the RBM and BSC equivalent dose are computed according to the path-lengths in the two sub-volumes.

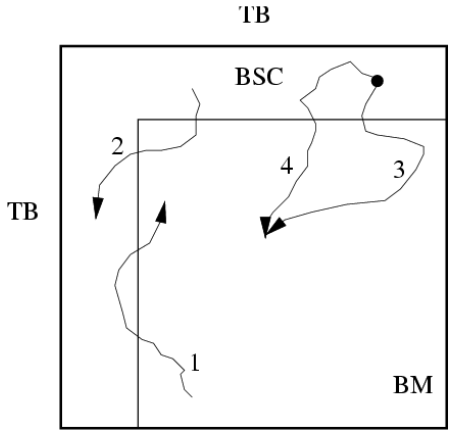

Figure 1b. This figure illustrates the problem of accurate computation of energy deposition for condensed history charged particle transport. Trajectory 1, although starting and ending in BM, may have portions of the curved path going through the BSC sub-volume. In a similar way, trajectory 2, which starts and ends in the BSC layer, has a portion traversing the BM sub-volume. Trajectories 3 and 4, although having the same intial and final position, have different path-lengths in the BSC and BM sub-volumes.

A more advanced method, based on a hinged step, was presented by Walters and Kawrakow (2007) in an investigation related to the faster computation of dose distributions in homogeneous phantoms irradiated by megavoltage external photon beams, a situation relevant in radiation treatment planning. An exact result can be obtained by forcing EGSnrc to go into analogue, single scattering mode, which

is possible by setting the „skin-depth“ parameter to a very large value. Because of the problem under consideration, the transport takes place in a micro voxel structure with 17.65-60 μm resolution and because EGSnrc does not allow condensed history steps to exceed the closest perpendicular distance to a region boundary, condensed history steps will be very short, never exceeding half the micro voxel size. Thus, one can anticipate that the simpler straight-line approach will yield accurate results. To verify this assumption, a single scattering calculation was performed for a few situations and in all cases agreement with the straight-line approach was observed within statistical uncertainties. This method is exact compared to methods sometimes applied which deposit all the energy for the step in one of the sub-volume based on checking the coordinates of only the initial position of the electron (Jokisch et al 2001). The error of this approximation could be small if one assumes that the electrons travel through the BSC volume coming uniformly from all directions. For whatever exposure condition this assumption may apply, here, for unidirectional incidence of the photons on the human body, this is certainly not the case because the flux of photo-electrons released in trabecular bone would occur preferably also in the direction of the incident photons.

2.5.2 BSC layer representation by systematically-periodically repeated micro clusters

The new energy deposition algorithm requires several other modifications in fax06_egsnrc. First, because now the BSC layer represents only a fraction of the volume of BM micro voxels adjacent to trabecular or cortical bone, the BM and BSC volumes must be calculated taking into account potential overlap of BSC layers at the different faces of a micro voxel. Second, because the BSC volume is no longer segmented a priori but determined at run time, the random selection of a micro matrix when entering a spongiosa voxel or when transferring the particle from one micro matrix to another, utilized in the FM paper, is no longer practical because the BM and BSC sub-volumes in micro voxels at the edges of a micro matrix would randomly change based on the random selection of the next micro

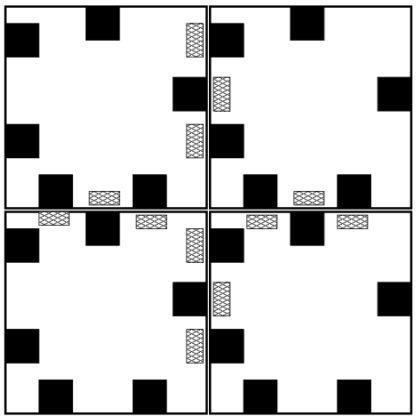

Figure 2a. Illustration of the problem of repeating the same micro-matrix structure. One of the four squares represents a n x n x n cluster of micro-matrices (2x2x2 in our case). The black rectangles represent areas of trabecular bone. When the n x n x n structure is repeated to the right and bottom (and also left and top, not shown here), areas of BSC indicated by the shaded rectangles are artifically created at the edges between the n x n x n clusters (in reality, one expects that the spongiosa structure will continuously change as one moves from left to right or top to bottom).

matrix. Thus, in all investigations reported here, a systematic-periodic approach was utilized. This approach is most easily understood by imagining that initially the entire space is filled with periodically repeating clusters of n_x x n_y x n_z micro matrices (2x2x2 or 3x3x3 in our case) and then the FAX06 phantom is superimposed replacing the micro matrices with the FAX06 macro voxels in all non-spongiosa regions.

Finally, a potential problem is the artificial generation of BSC layers when repeating a micro cluster periodically. This is illustrated in figure 2a. Each of the four squares of this figure represents one cluster of n_x x n_y x n_z micro matrices, with the black areas indicating trabecular bone. When a cluster is repeated periodically to the right and bottom (and also left and top, front and back, not shown) the areas indicated by the shaded rectangles will be considered BSC layers. This is considered to be a potential problem because in reality one would expect a continuous variation of the spongiosa structures as opposed to the drastic change from right to the left, bottom to top, and front to back face of a micro cluster caused by the periodic repetition. To investigate this issue, $2n_x$ x $2n_y$ x $2n_z$ clusters were created from the n_x x n_y x n_z clusters by combining copies mirrored at the xy-, xz- and yz-planes as indicated in figure 2b. When repeating these new clusters periodically, there are no artificially generated BSC volumes because now the left/top/front edge of a cluster is exactly the same as the

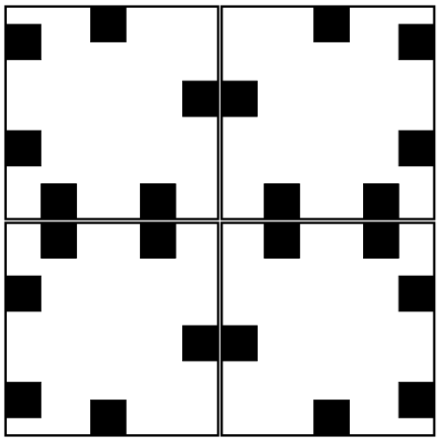

Figure 2b. Illustration of a 2n x 2n x 2n cluster of micro matrices obtained from a n x n x n cluster by combining copies of the n x n x n cluster mirrored on the xy-, xz- and yz-planes. Note that now there are no artificially generated BSC regions. Also note that there will be no artificial BSC regions when repeating this 2n x 2n x 2n structure because now the left/right, top/bottom and front/back faces are identical.

right/bottom/back edge. Calculations of the BSC and RBM equivalent doses with these $2n_x$ x $2n_y$ x $2n_z$ clusters for the micro matrices in the first 3 rows of Table 3 showed agreement within statistical uncertainties (0.3% or better) with the corresponding n_x x n_y x n_z clusters. Thus, for the remainder of the paper only results calculated with the clusters mentioned in table 3 will be reported.

3. Results and Discussions

Whole-body irradiations for parallel frontal incidence (AP) have been simulated with the fax06_egsnrc code for photon energies between 10 keV and 10 MeV. The minimal cortical bone thickness in the FAX06 skeleton is 1.2 mm. This implies that electrons moving in regions outside the skeleton must have at least 550 keV kinetic energy in order to enter a spongiosa voxel after passing through the cortical region. Thus, cut-off energies were set to 2 keV for photons, 550 keV for electrons in tissues

outside the skeleton and 5 keV for electrons in the skeletal tissues. All EGSnrc transport parameters and cross section options were left at their default values, which are set to achieve the best accuracy EGSnrc is capable of. The number of primary photons varied between 5 and 20 million to achieve a statistical error of less than 1% for the RBM and BSC equivalent dose in the whole skeleton for incident photon energies above 30 keV. For 30 keV and smaller energies the statistical error for the BSC equivalent dose was 5% or less.

3.1 BSC equivalent dose for different voxel resolutions

Figure 3 presents conversion coefficients (CCs) between the BSC equivalent dose for a layer thickness of 10 μm and air kerma free-in-air. Results are for anterior-posterior (AP) incidence as a function of the photon energy for cubic voxel resolutions of 17.65, 30 and 60 μm based on modified vertebral TBVFs. The extrapolated BSC equivalent dose from the FM paper is also included for comparison. The figure clearly shows that the interpolation method, while providing a reasonable first estimate for the BSC equivalent dose, is only accurate to within about 10%.

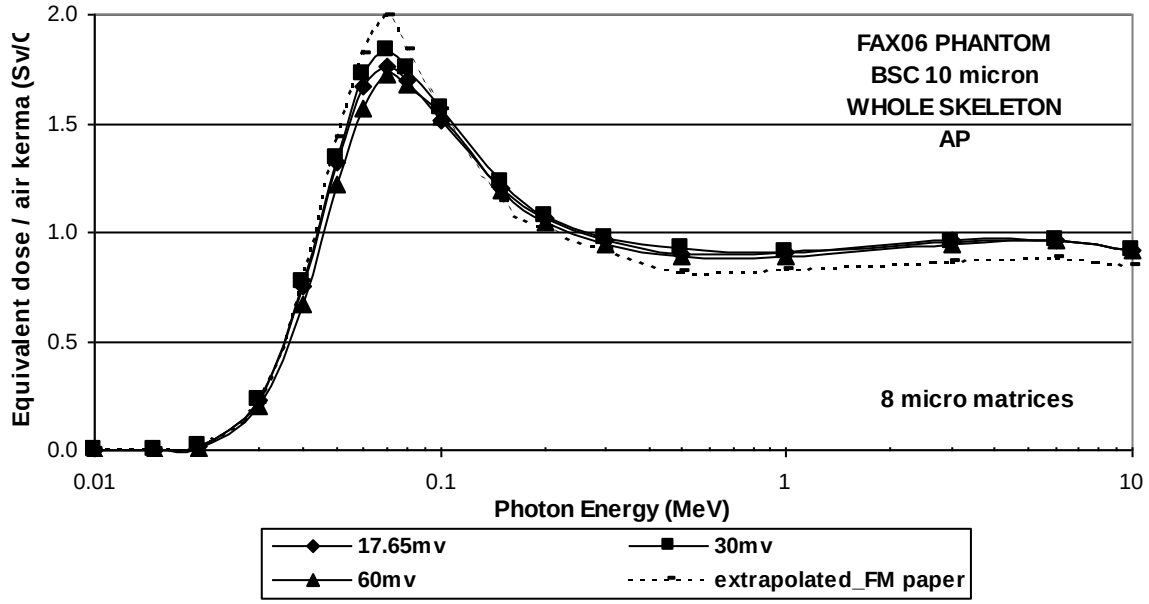

Figure 3. BSC equivalent dose per air kerma free-in-air in the FAX06 skeleton as a function of the photon energy and AP incidence for the same TBVFs but with different cubic voxel resolutions

Table 4. Percentage differences between CCs shown in figure 3

E MeV	30 / 17.65 %	30 / 60 %	E MeV	30 / 17.65 %	30 / 60 %
0.02	6.3	30.8	0.15	2.3	2.7
0.03	0.4	14.5	0.20	0.6	3.0
0.04	1.6	14.1	0.30	0.8	2.4
0.05	2.0	10.4	0.50	2.3	3.2
0.06	3.5	10.1	1.00	0.4	1.9
0.07	4.0	6.7	3.00	-0.8	0.6
0.08	3.1	4.2	6.00	-0.1	-0.4
0.10	3.2	2.5	10.00	0.3	0.3

The CCs for the three resolutions often show differences greater than the combined statistical uncertainties, especially in the energy range below 150 keV. Voxel effects can be ruled out, as already discussed in the FM paper, but also because of the alternating behaviour of the CCs. The greatest values can be observed for 30 μm voxel resolution, followed by 17.65 μm and by 60 μm. Voxel effects would cause continuous alterations when the voxel resolution is either increasing or decreasing. Percentage differences per energy point between the 30 μm CC and the two other CCs are listed in table 4. Below 100 keV the differences between 30 and 60 μm voxel resolution are much greater than those between 30 and 17.65 μm voxel resolution, although the differences between the voxel resolutions are roughly a factor of two for both cases. At this stage, a conclusive explanation for this observation is difficult because, apart from different voxel resolutions, the three clusters are also based on different bone sites segmented with different methods.

3.2 BSC equivalent dose for the same voxel resolution and with original TBVFs

Figure 4 presents CCs for the micro sets 26o1 and 26o2 for a cubic voxel resolution of 26 μm and for original TBVFs in the spongiosa of the spine, the long bones and the pelvis. In other words, in figure 4, the TBVFs of all bones in the two micro sets are equal, except for the two spines which show a difference of 3.8% between their TBVFs according to table 3.

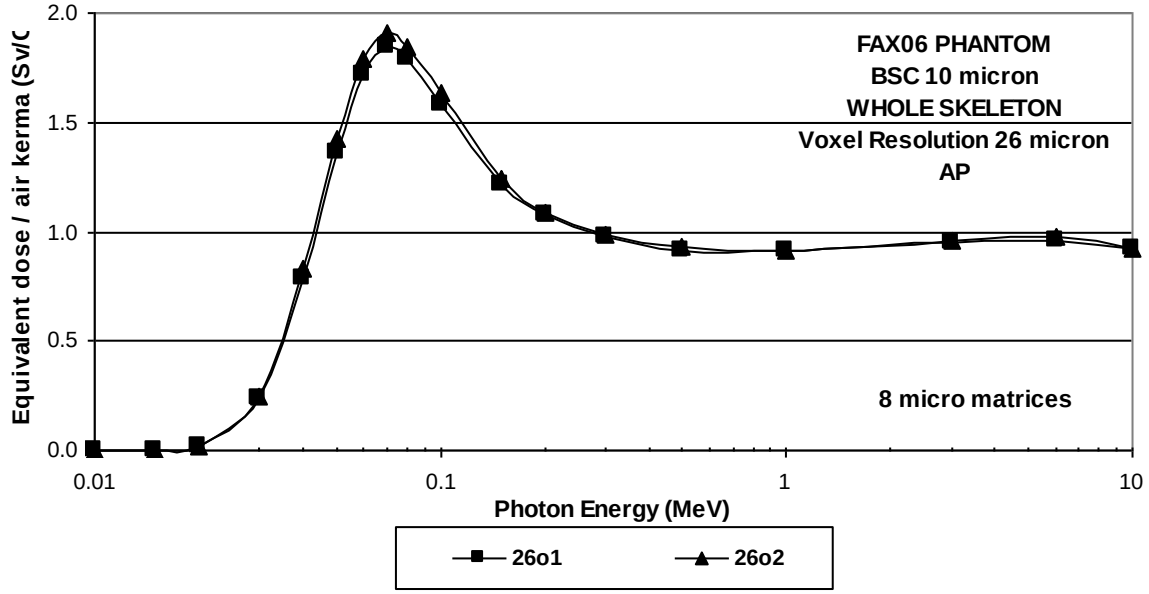

Figure 4. BSC equivalent dose per air kerma free-in-air in the FAX06 skeleton as a function of the photon energy and AP incidence with the same cubic voxel resolution but for different TBVFs.

Below 150 keV also the two CCs for the 26o1 and 26o2 micro sets presented in figure 4 show differences greater then their combined statistical errors. These differences, listed in table 5 as function of the incident photon energy, are smaller than those seen between 30 and 60 μm voxel resolution in table 4, but they are of the same order as, and often even larger than, the 30 / 17.65 μm differences. Figure 4 suggests that these differences are caused by the different TBVFs for the spines, because voxel resolution, segmentation method and the TBVFs for all the other bones are the same for the two CCs. To see if this explains the whole difference, one has to investigate these CCs for equal TBVFs.

Table 5. Percentage differences between CCs shown in figure 4

E MeV	26o1 / 26o2 %	E MeV	26o1 / 26o2 %
0.02	5.9	0.15	2.6
0.03	4.6	0.20	0.5
0.04	5.3	0.30	0.9
0.05	4.6	0.50	0.8
0.06	4.0	1.00	-0.3
0.07	3.5	3.00	0.9
0.08	3.1	6.00	1.1
0.10	3.1	10.00	-0.1

3.3 BSC equivalent dose for the same voxel resolution and TBVFs

Figure 5 presents the CCs for the micro sets 26mv1 and 26mv2 for a cubic voxel resolution of 26 μm, for the same segmentation method and for equal TBVFs in all bones but still derived from two different vertebrae of the same donor.

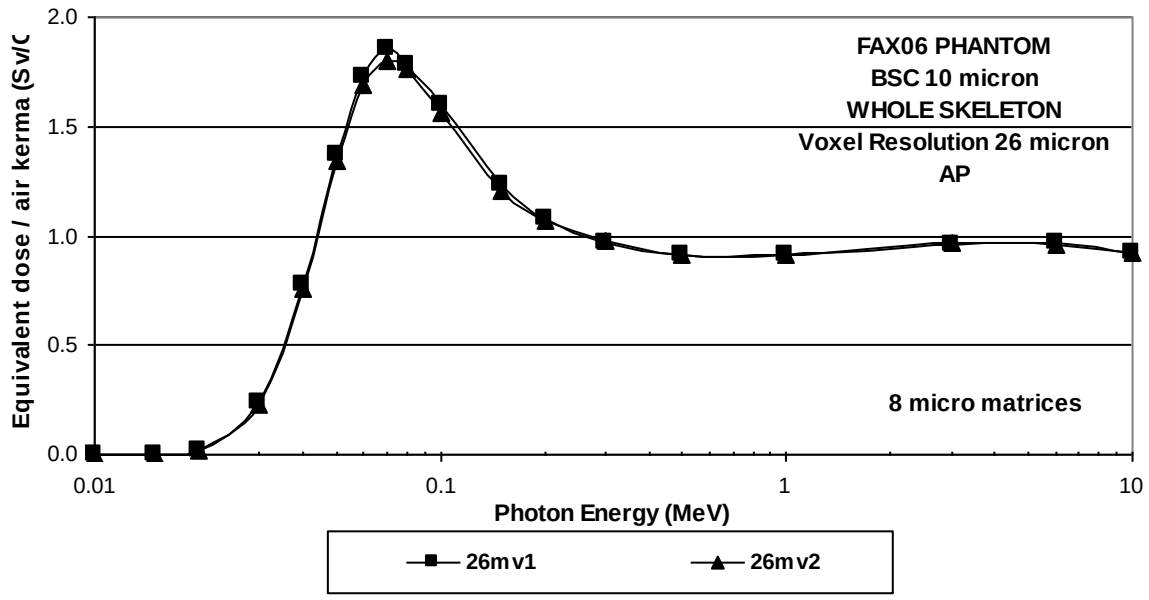

Figure 5. BSC equivalent dose per air kerma free-in-air in the FAX06 skeleton as a function of the photon energy and AP incidence with the same cubic voxel resolution and TBVFs, but derived from different vertebrae of the same donor.

The percentage differences per energy point between the two CCs can be seen in table 6. They are slightly smaller than those listed in table 5, which suggests that equal TBVFs are responsible for this small decrease. However, the differences one observes are still greater than the combined statistical errors, although the two micro sets have the same voxel resolution, the same TBVFs, come from the same donor and have been segmented by the same method. Similar percentage differences were found for the CCs 26mv1p and 26mv2p (not shown), where the 20% TBVF for the pelvis was derived from the original images of the iliac crest and not from the corresponding vertebrae. Perhaps the number of micro matrices in the cluster is not large enough to capture the essential spongiosa structure? This hypothesis would suggest that a larger cluster would lead to a decrease of differences between micro sets obtained in exactly the same way but from different bone sample.

Table 6. Percentage differences between CCs shown in figure 5

E MeV	26mv1 / 26mv2 %	E MeV	26mv1 / 26mv2 %
0.02	-5.9	0.15	2.2
0.03	2.6	0.20	0.1
0.04	2.9	0.30	-0.6
0.05	2.7	0.50	0.0
0.06	2.3	1.00	-0.3
0.07	2.9	3.00	-1.1
0.08	1.0	6.00	0.5
0.10	2.2	10.00	0.4

3.4 BSC equivalent dose for clusters with 27 micro matrices

Figure 6 presents the CCs for the micro sets 26mv1_27 and 26mv2_27 for a cubic voxel resolution of 26 μm and for equal TBVFs in all bones, derived from two different vertebrae of the same donor but now with 3 x 3 x 3 = 27 micro matrices in the clusters, i.e. a larger coherent volume of spongiosa has been extracted from the vertebral images B2026 and B2126 compared to the clusters based on 8 micro matrices.

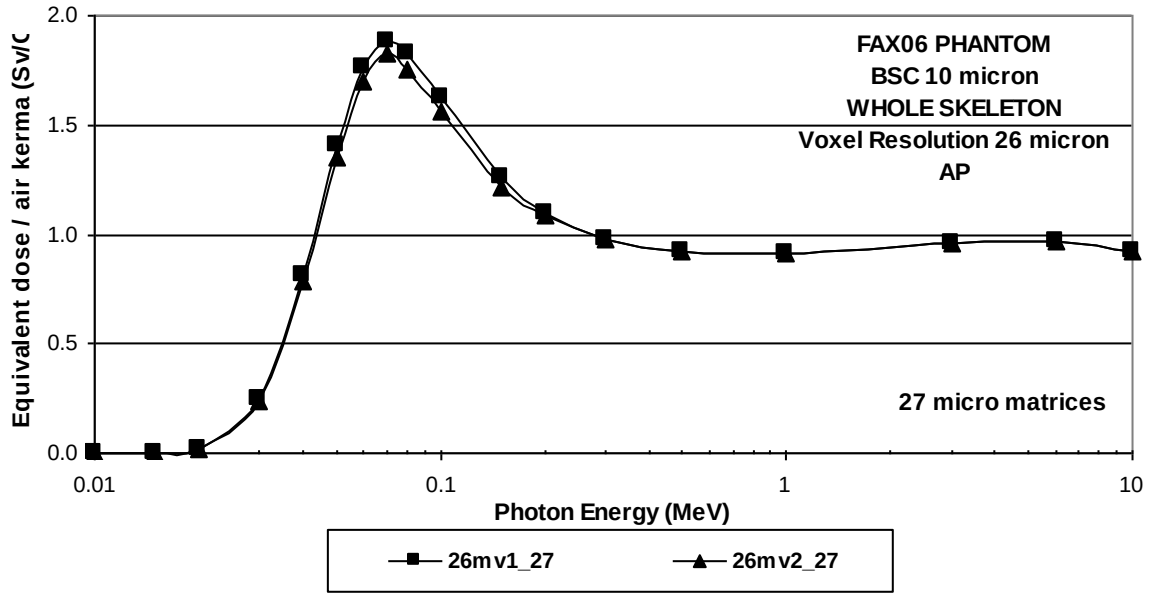

Figure 6. BSC equivalent dose per air kerma free-in-air in the FAX06 skeleton as a function of the photon energy and AP incidence with the same cubic voxel resolution and TBVFs, derived from different vertebrae of the same donor, but with 27 micro matrices in the clusters.

Table 7. Percentage differences between CCs shown in figure 6

E MeV	26mv1_27 / 26mv2_27 %	E MeV	26mv1_27 / 26mv2_27 %
0.02	0.0	0.15	3.7
0.03	3.8	0.20	0.6
0.04	4.0	0.30	-0.1
0.05	4.1	0.50	0.0
0.06	3.8	1.00	0.0
0.07	3.0	3.00	0.3
0.08	4.2	6.00	0.5
0.10	4.6	10.00	0.0

As for the percentage differences, table 7 presents the same pattern as already observed in table 6 for the data of figure 5, which shows basically no significant differences above 150 keV where the photo-electric effect is negligible, however clear differences greater than the combined statistical errors for incident photon energies below 150 keV.

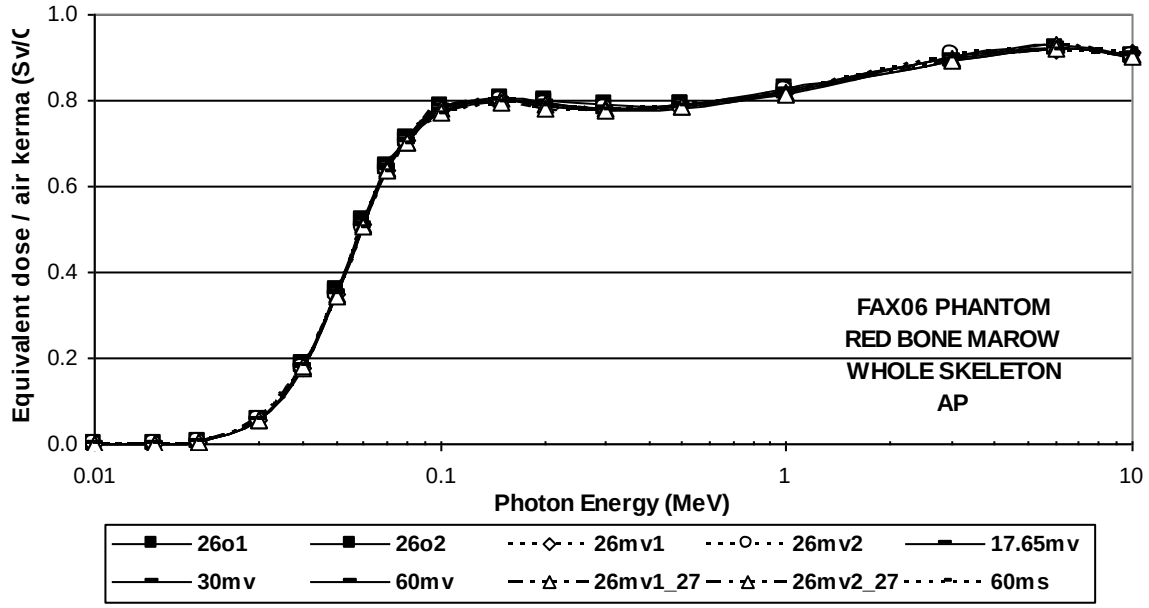

Figure 7. RBM equivalent dose per air kerma free-in-air in the FAX06 skeleton as a function of the photon energy and AP incidence for the micro sets 17.65mv, 30mv, 60mv, 60ms, 26o1, 26o2, 26mv1 and 26mv2 with 8 micro matrices, and 26mv1_27 and 26mv2_27 with 27 micro matrices.

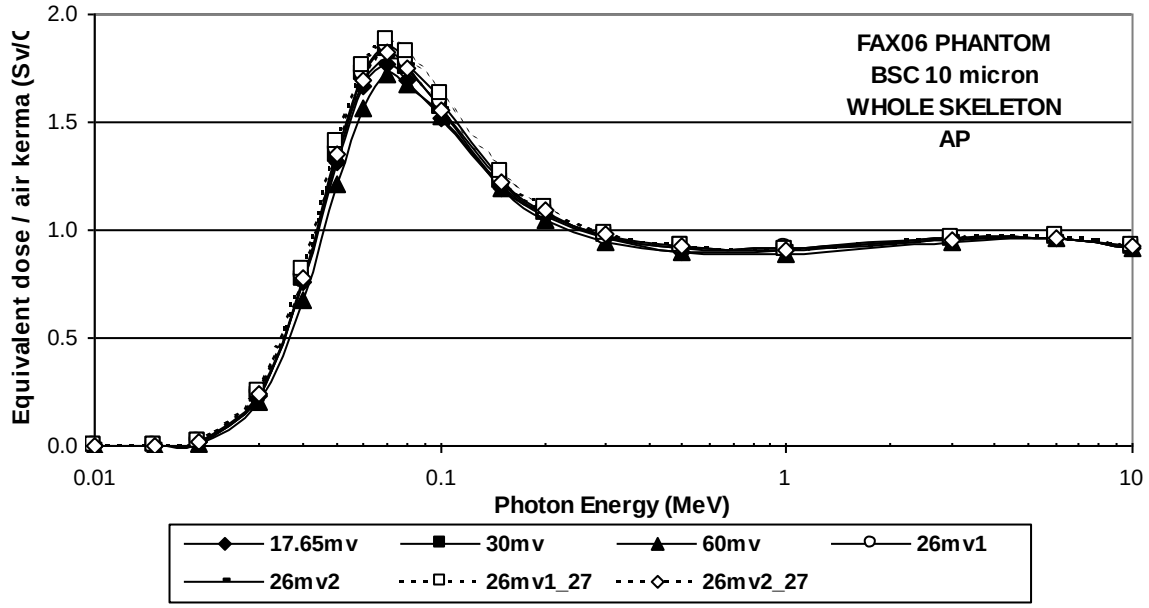

Figure 8. BSC equivalent dose per air kerma free-in-air in the FAX06 skeleton as a function of the photon energy and AP incidence for all vertebra-based micro sets shown in figures 4, 5 and 6

Figure 7 presents CCs between the RBM equivalent dose and air kerma free-in-air for AP incidence as a function of the photon energy for the micro sets shown in table 3, except for 26mv1p and 26mv2p. All RBM CCs agree within the combined margin of their statistical errors. It seems that apart from voxel resolution, TBVF, segmentation method and donor, the specific trabecular bone structure of the bone site may not influence the RBM, but indeed the BSC equivalent dose, which is reinforced once more in the summary figure 8, which combines all BSC results presented so far.

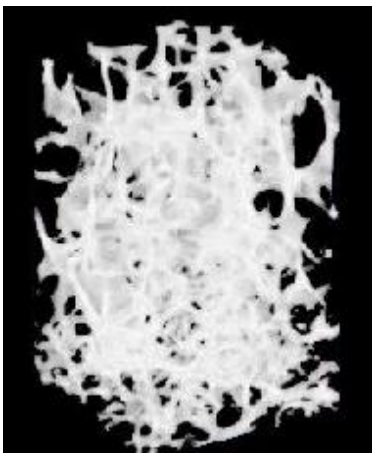

Figure 9a. 3D-image of specimen B2026 modified to 12% TBVF

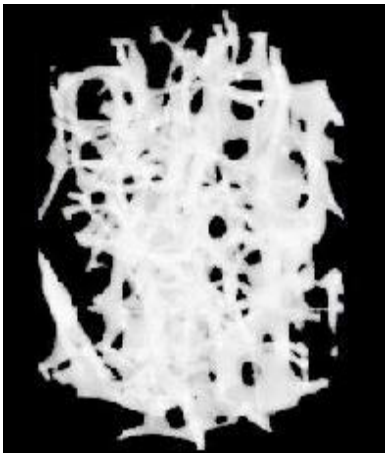

Figure 9b. 3D-image of specimen B2126 modified to 12% TBVF

Figures 9a and 9b show 3D-images extracted from the two vertebrae B2026 and B2126 after having been modified to a TBVF of 12%. The two specimens come from the same individual, have been segmented with the same method, scanned with the same voxel resolution, have the same TBVF, but nevertheless show clearly different trabecular bone structures, with thickness and orientation of the trabeculae visibly different in the two images. For incident photon energies up to 150 keV, the BSC equivalent dose is strongly influenced by the flux of secondary photo-electrons released by photon interactions in trabecular bone, which then enter the marrow cavities. The ranges of such electrons are short and therefore the dose enhancement one observes near a trabecular bone surface quickly disappears at larger distances. Thus, one can expect that by increasing the BSC layer thickness the differences seen in figures 5 and 6 will decrease. Additionally, the RBM equivalent dose should be basically independent from the specific trabecular bone structure for all incident photon energies, at least as long as the RBM equivalent dose is calculated as the average equivalent dose to the remaining marrow weighted by the cellullarity factor. This is exactly what figure 7 demonstrates. According to this interpretation of the differences observed for the BSC equivalent dose in figures 4, 5 and 6 or 8, if the thickness for the bone endosteum would be raised to 50 μm, one should see a decrease or perhaps even a disappearance of the dependence of the BSC equivalent dose on the trabecular bone structure.

3.5 BSC equivalent dose for 50 μm layer thickness

Table 8. Percentage differences between CCs shown in figure 10

E	mv10 / ms10	mv50 / ms50	E	mv10 / ms10	mv50 / ms50
MeV	%	%	MeV	%	%
0.02	27.8	23.1	0.15	1.4	0.8
0.03	8.7	5.6	0.20	1.7	1.5
0.04	5.1	2.1	0.30	1.8	1.1
0.05	4.1	1.8	0.50	1.7	1.6
0.06	2.3	0.9	1.00	1.3	0.8
0.07	2.1	0.6	3.00	0.9	1.1
0.08	1.4	0.1	6.00	0.1	0.1
0.10	2.1	0.7	10.00	0.1	0.2

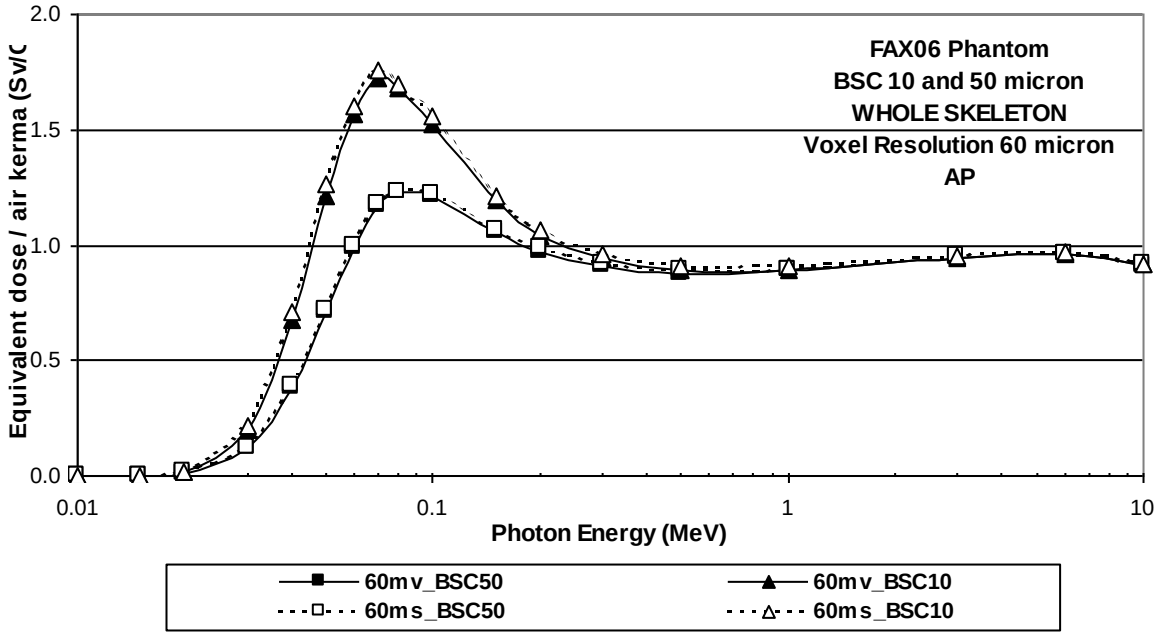

Figure 10. BSC equivalent dose per air kerma free-in-air in the FAX06 skeleton as a function of the photon energy and AP incidence for the micro sets 60mv and 60ms with BSC thickness of 10 and 50 μm.

Figure 10 presents CCs between the BSC equivalent dose and air kerma free-in-air for AP incidence as a function of the photon energy for the micro sets 60mv and 60ms calculated for 10 and 50 μm thickness of the BSC layer. The percentage differences decrease as expected when the BSC thickness is raised from 10 to 50 μm, which can also be observed from the comparison shown in table 8, where mv10/ms10 and mv50/ms50 represent the BSC equivalent dose differences between the vertebra-based (mv) and the skull-based (ms) micro cluster for 10 and 50 μm BSC thickness, respectively. In other words: Similar to the observations already made for the RBM equivalent dose, increasing the BSC thickness from 10 to 50 μm would make also the BSC equivalent dose basically independent from the specific properties of the trabeculae for external exposure to photons, if one can accept variations of up to 2% for energies above 30 keV. For the 10 μm thickness these variations would be up to 5%.

3.6 Stylized spongiosa

Efforts have been made to develop adult human phantoms and to calculate skeletal tissue masses based on recommendations published by the ICRP (Kramer et al 2003, 2004, 2006a, Zankl et al 2007, Watchman et al 2007b, Schlattl et al 2007), some of which eventually will become ICRP reference phantoms or reference masses. The interesting question is: How will human reference spongiosa be defined for the purposes of skeletal dosimetry? Will it be the trabecular bone structure of a specific bone specimen, such as B0160 or S0117? And once reference TBVFs have been determined, how will they be realized in a trabecular bone specimen? By the method used in this study, for example? While it is relatively easy to design form, shape and volume of a reference liver, for example, it seems rather complicated to perform a similar task by modifying the spongiosa of lumbar vertebrae from different bone sites or donors in order to design a reference spongiosa for vertebral bodies. Also, considering that for given TBVFs the results of this investigation demonstrate that the RBM equivalent dose is independent of the specific trabecular bone structure, segmentation method and details of image acquisition, whereas the BSC equivalent dose depends indeed probably on all these parameters, thus suggesting that any “reference spongiosa” attempt will always imply BSC equivalent doses not more accurate than the 2-5% variations observed here, why then not model human spongiosa as stylized spongiosa, i.e. having cavities with a well defined volume, shape and spatial distribution?

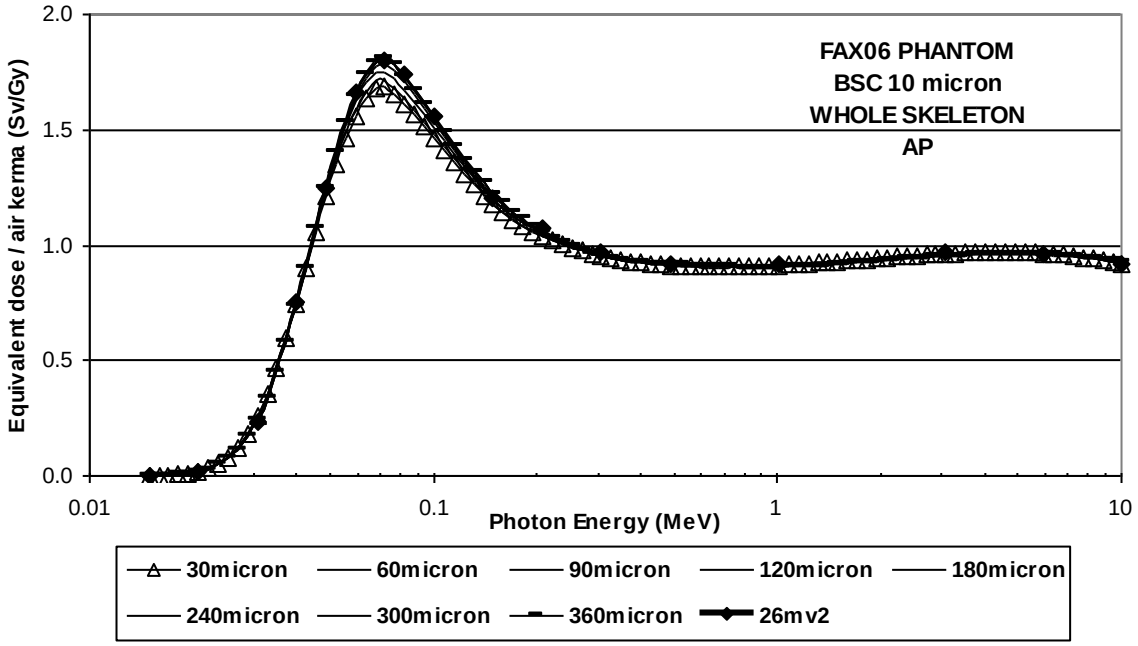

Figure 11. BSC equivalent dose for 10 μm layer thickness per air kerma free-in-air in the FAX06 skeleton as a function of the photon energy and AP incidence for micro set 26mv2 and for stylized micro sets with cubic cavity sizes between 30 and 360 μm.

To investigate such a possibility, artificial micro clusters were created by randomly placing rectilinear marrow cavities within trabecular bone until the desired TBVF was reached. Different sizes of the randomly placed cubic bone marrow cavities were used to obtain clusters with 8 micro matrices ranging between 30 μm and 360 μm cubic cavity sizes. Figure 11 shows the 10 μm BSC equivalent dose for these stylized spongiosas and for comparison also the CC 26mv2 from figure 4.
Two very interesting observations can be made. First, within a margin of 2% the BSC equivalent dose becomes basically independent of the cavity size for cubic cavities of 120 μm or larger, i.e. for cavity sizes typically found in human spongiosa, and the "stylized" results are absolutely comparable to the data based on a real bone specimen. Second, the differences between the BSC equivalent doses for cubic cavity sizes of 120 μm or greater computed with these artificial micro clusters are also comparable to the differences between BSC equivalent doses observed for the CCs of the real bone specimens shown in figures 4 to 6. Thus, a stylized spongiosa made of cavities with well-defined volumes, shape and spatial distribution may serve as a reference microstructure for skeletal dosimetry. It is worth noting that a similar approach has been made for skeletal dosimetry for internal exposure to electrons by Gersh et al (2006) where the marrow cavities had the form of spheres.

4. Conclusions

With respect to the purposes of this study mentioned above, the following conclusions can be drawn:

a) The algorithm introduced here, allows for a direct calculation of the BSC equivalent dose in sub-volumes of micro voxels based on the partitioning of the linear electron step length according to the distances travelled in the BSC and BM sub-volumes, respectively. The algorithm can be adapted to any Monte Carlo investigation which has to score energy or any other quantity in sub-volumes of voxels. For example, to the calculation of the skin equivalent dose in a thin layer on the body's surface, which is often smaller than the thickness of a voxel.

b) The assumptions made about the distribution of the BSC in the human skeleton led to the application of the systematic-periodic (SP) instead of the random (R) selection of micro matrices from the cluster in order to preserve coherently the structure of the spongiosa for the BSC equivalent dose calculation, especially at the boundaries with cortical bone. Both selection modes had been introduced earlier (Kramer et al 2006b). Increasing the number of micro matrices from 8 to 27 did not change the results for the equivalent doses to the RBM and the BSC. Therefore, the 8 SP cluster method will be the method of choice for future studies in skeletal dosimetry.

c) The results for the whole-body RBM equivalent dose for external exposure to photons presented in this study have shown that this quantity does not depend on the voxel resolutions, segmentation methods, and bone sites used here, thereby confirming an observation already made in the FM paper. Additionally this study has demonstrated that the whole-body RBM equivalent dose also does not depend on moderate variations of the TBVFs. This may look differently, of course, if one considers in the future partial body exposures, for example, of the pelvis for PA incidence with the original TBVF of 7.4% on the one hand and with the modified TBVF of 20% on the other hand.

d) Because of the thickness of only 10 μm and the close proximity of the BSC to the surface of trabecular bone, the BSC equivalent dose is in principle much more sensitive to the properties or changes of voxel resolution, segmentation methods and bone site-specific trabecular bone structure than the RBM equivalent dose. Although a clear dependence of the BSC equivalent dose on the voxel resolution was not observed in this study, a corresponding investigation would require μCT images of one and the same trabecular bone sample scanned with different voxel resolutions. The same argument applies to the segmentation method. Such images are currently not available.

e) In this study, it was possible to observe a "trabecular bone structure (TBS) effect" for the BSC equivalent dose, which can be interpreted as bone site-specific influence of the trabeculae on the flux of photo-electrons into the marrow cavities even if voxel resolution, segmentation method and TBVFs are equal. It was possible to demonstrate that for a given bone site this TBS effect depends on the thickness of the BSC layer. In particular it was shown that the TBS effect almost disappears if the BSC reference thickness would be raised to 50 μm.

f) Although the use of μCT images of real trabecular bone samples will surely continue for some time, it is perhaps nevertheless worthwhile looking into the issue of "stylized spongiosa" for the purposes of reference dosimetry. Preliminary results have been shown in this study, yet more investigations also for the RBM and other exposure conditions are necessary. When human phantoms and skeletal tissue masses are getting normalized, it is difficult to imagine that reference skeletal dosimetry in the area of radiation protection would be based on specific bone samples from a specific individual with arbitrary TBVFs.

5. Acknowledgement

The authors want to express their gratitude to Dr. J. Bauer from the Institut für Röntgendiagnostik of the Technische Universität Muenchen, Germany, to Dr. P. Salmon from Skyscan Corporation, Belgium, to Dr. D. Rajon from the Department of Neurological Surgery and to Prof. W. Bolch, Director at the Advanced Laboratory for Radiation Dosimetry Studies (ALRADS), both from the University of Florida, USA for the μCT images they made available for this study. Special thanks go to Dr.A.Kramer for reviewing the paper prior to submission from a medical point of view.

The authors would also like to thank the Conselho Nacional de Desenvolvimento Científico e Tecnológico (CNPq) and the Fundação de Amparo à Ciência do Estado de Pernambuco (FACEPE) for the financial support.

6. References

Berger M J 1963 Monte Carlo Calculation of the penetration and diffusion of fast charged particles, *Methods in Computational Physics*, Alder B, Fernbach S and Rotenberg M (edts.), Academic, New York, 135-215.

Bauer J S, Issever A S, Fischbeck M, Burghardt A, Eckstein F, Rummeny E J, Majumdar S, Link T M 2004 Multislice-CT for structure analysis of trabecular bone - a comparison with micro-CT and biomechanical strength *Rofo Fortschr Geb Rontgenstr Neuen Bildgeb Verfahr* **176** (5) 709-718

Bolch W E, Patton P W, Rajon D A, Shah A P, Jokisch D W and Inglis B A 2002 Considerations of Marrow Cellularity in the 3-Dimensional Dosimatric Models of the Trabecular Skeleton *J Nucl Med* **43**, No.1, 97- 108

Bolch W E, Shah A P, Watchman C J, Jokisch D W, Patton P W, Rajon D A, Zankl M, Petoussi-Henss N and Eckerman K F 2007 Skeletal Absorbed Fractions for Electrons in the Adult Male: Considerations of a Revised 50-mm Definition of the Bone Endosteum *Rad.Prot.Dos*. **127** 169-173

Gersh J A, Dingfelder M and Toburen L H 2006 Monte Carlo Modelling of Energy Deposition in Trabecular Bone *Rad.Prot.Dos*. Vol.122, No.1-4, pp.549-550

ICRP 1979 Limits for Intakes of Radionuclides by Workers *ICRP Publication 30* (Oxford: Pergamon)

ICRP 1991 1990 Recommendations of the International Commission on Radiological Protection *ICRP Publication 60* (Oxford: Pergamon)

ICRP 1995 Basic Anatomical and Physiological Data for use in Radiological Protection: The Skeleton. *ICRP Publication 70* (Oxford: Pergamon)

ICRP 2002 Basic Anatomical and Physiological Data for Use in Radiological Protection: Reference Values *ICRP Publication 89* Ann. ICRP 32 (3-4) Elsevier Science Ltd., Oxford.

ICRP 2007 Recommendations of the International Comission on Radiological Protection *ICRP Publication 103* Ann. ICRP 37 (2-3) Elsevier Science Ltd., Oxford (in press)

ICRU 1989 Tissue Substitutes in Radiation Dosimetry and Measurement *ICRU Report No. 44* International Commission On Radiation Units And Measurements, Bethesda, MD, USA

ICRU 1992 Photon, Electron, Proton and Neutron Interaction Data for Body Tissues *ICRU Report No. 46* International Commission On Radiation Units And Measurements, Bethesda, MD, USA

Jokisch D W, Patton P W, Inglis B A, Bouchet L G, Rajon D A, Rifkin J and Bolch W E 1998 NMR Microscopy of Trabecular Bone and its Role in Skeletal Dosimetry *Health Physics* **75**(6), 584-596

Jokisch D W, Bouchet L G, Patton P W, Rajon D A and Bolch W E 2001 Beta-particle dosimetry of the trabecular skeleton using Monte Carlo transport within 3D digital images *Med.Phys.* **28** (7), 1505-1518

Kawrakow I 2000a Accurate condensed history Monte Carlo simulation of electron transport. I. EGSnrc, the new EGS4 version, *Med.Phys.* **27**, 485-498

Kawrakow I 2000b Accurate condensed history Monte Carlo simulation of electron transport. II. Application to ion chamber response simulations, *Med.Phys.* **27**, 499-513

Kawrakow I and Rogers D.W.O. 2003 The EGSnrc code system: Monte Carlo simulation of electron and photon transport, *NRC Report PIRS-701*

Kawrakow I 2006 Version V4-r2-2-3 of the EGSnrc code system *http://www.irs.inms.nrc.ca/EGSnrc/EGSnrc.html*

Kramer R, Vieira J W, Khoury H J, Lima F R A and Fuelle D 2003 All About MAX: a Male Adult voXel Phantom for Monte Carlo Calculations in Radiation Protection Dosimetry, *Phys. Med. Biol*., **48**, No. 10, 1239-1262

Kramer R, Vieira J W, Khoury H J, Lima F R A, Loureiro E C M, Lima V J M and Hoff G 2004 All about FAX: a Female Adult voXel Phantom for Monte Carlo Calculation in Radiation Protection Dosimetry, *Phys. Med. Biol.* **49**, 5203-5216

Kramer R, Khoury H J, Vieira J W and Lima V J M 2006a MAX06 and FAX06: Update of two adult human phantoms for radiation protection dosimetry *Phys. Med. Biol.* **51** 3331-3346

Kramer R, Khoury H J, Vieira J W and Kawrakow I 2006b Skeletal dosimetry in the MAX06 and the FAX06 phantoms for external exposure to photons based on vertebral 3D-microCT images *Phys.Med.Biol.* **51** 6265-6289

Nelson W R, Hirayama H and Rogers D W O 1985 The EGS4 Code System *SLAC-265*, Stanford Linear Accelerator Center, Stanford University, Stanford, CA,USA

Patton P W, Rajon D A, Shah A P, Jokisch D W, Inglis B A and Bolch W E 2002 Site-specific variability in trabecular bone dosimetry: Considerations of energy loss to cortical bone *Med.Phys.* **29** (1), 6-14

Rajon D A, Jokisch D W, Patton P W, Shah A P, Watchman C J and Bolch W E 2002 Voxel effects within digital images of trabecular bone and their consequences on chord-length distribution measurements *Phys.Med.Biol.* **47** 1741-1759

Rajon D A, Pichardo J C, Brindle J M, Kielar K N, Jokisch D W, Patton P W and Bolch W E 2006 Image segmentation of trabecular spongiosa by visual inspection of the gradient magnitude *Phys.Med.Biol* **51** 4447-4467

Richardson R B, Nie H L and Chettle D R 2007 Monte Carlo Simulation of Trabecular Bone Remodelling and Absorbed Dose Coefficients for Tritium and ^{14}C *Rad Prot Dos* **127** 1-4 158-162

Salmon P 2006 personal communication *Skyscan Corporation*, 2630 Aartselaar, Belgium

Schlattl H, Zankl M and Petoussi-Henss N 2007 Organ dose conversion coefficients for voxel models of the reference male and female from idealized photon exposures *Phys.Med.Biol* **52** 2123-2145

SCION Image for WINDOWS 2000 Scion Corporation, www.scioncorp.com

Shah A P, Patton P W, Rajon D A and Bolch W E 2003 Adipocyte Spatial Distributions in Bone Marrow: Implications for Skeletal Dosimetry Models *J Nucl Med* **44**, No. 5, 774-783

Shah A P, Rajon D A, Jokisch D W, Patton P W and Bolch W E 2005a A Comparison of Skeletal Chord-Length Distributions in the Adult Male *Health Phys.* **89** (3): 199-215

Shah A P, Jokisch D W, Rajon D A, Watchman C J, Patton P W and Bolch W E 2005b Chord-based versus voxel-based methods of electron transport in the skeletal tissues *Med.Phys.* **32** (10), 3151-3159

Shah A P, Bolch W E, Rajon D A, Patton P W and Jokisch D W 2005c A Paired-Image Radiation Transport Model for Skeletal Dosimetry *J Nucl Med* **46**, No.2, 344-353

Shah A P, Rajon D A, Patton P W, Jokisch D W and Bolch W E 2005d Accounting for beta-particle loss to cortical bone via paired-image radiation transport (PIRT) *Med.Phys.* **32** (5), 1354-1366

Spiers F W 1969 Transition-Zone Dosimetry *Radiation Dosimetry* Volume III: *Sources, Fields, Measurements and Applications*, 2nd edition, edited by F H Attix and E Tochilin, Academic Press, New York and London

Spiers F W 1974 Radionuclides and bone – from ^{226}Ra to ^{90}Sr *Br.J.Radiol.* **47**, No 564, 833-844

Walters B R B and Kawrakow I 2007 A "HOWFARLESS" option to increase efficiency in homogeneous phantom calculations with DOSXYZnrc, *Med. Phys.* **34** No.10, 3794-3807

Watchman C J, Bourke V A, Lyon J R, Knowlton A E, Butler S L, Grier D D, Wingard J R, Braylan R C and Bolch W E 2007a Spatial Distribution of Blood Vessels and $CD34^+$ Hematopoietic Stem and Progenitor Cells Within the Marrow Cavities of Human Cancellous Bone *J Nucl Med* **48**: 645-654

Watchman C J, Hasenauer D and Bolch W E 2007b Derivation of site-specific skeletal masses within the current ICRP age series *Phys.Med.Biol* **52** 3133-3150

Zankl M, Eckerman K F and Bolch W E 2007 Voxel-Based Models Representing the Male and Female ICRP Reference Adult – The Skeleton *Rad.Prot.Dos.* Advanced Access published June 2, 2007